Shell-model study of ^{40}Ca with the 56-MeV $(\vec{d}, p)$ reaction

Y. Uozumi, N. Kikuzawa, T. Sakae, and M. Matoba
Department of Nuclear Engineering, Kyushu University, Fukuoka 812, Japan

K. Kinoshita,* T. Sajima,† and H. Ijiri
Graduate School of Engineering and Sciences, Kyushu University, Kasuga 816, Japan

N. Koori
Faculty of Integrated Arts and Sciences, Tokushima University, Tokushima 770, Japan

M. Nakano and T. Maki
University of Occupational and Environmental Health, Kitakyushu 807, Japan
(Received 6 July 1993)

Single-particle states in ^{41}Ca have been investigated through the ^{40}Ca$(\vec{d}, p)^{41}$Ca reaction with polarized deuterons of $E_d = 56$ MeV. Angular distributions of differential cross sections and vector analyzing powers were measured for 91 transitions up to 9.7-MeV excitation energy by using a magnetic spectrograph. Analyses of these data were performed to determine j^π and C^2S of single-particle levels with zero-range distorted-wave Born approximation calculations using the adiabatic approximation. The occupation probabilities and the single-particle energies in ^{40}Ca were extracted for the valence $(2p - 1f)$ and $(2s - 1d)$ shells with including previous (p, d) data. The results on these quantities show good agreement with theoretical expectations.

PACS number(s): 21.10.Jx, 21.60.Cs, 25.45.Hi, 27.40.+z

I. INTRODUCTION

In recent decades, there has been a renewal of interest in nuclear spectroscopy in order to solve problems such as the missing strength in the Gamow-Teller giant resonance (GTGR) [1], which has been one of the most popular topics in nuclear physics, depletion of single-particle strength [2] near the Fermi surface, and ground state correlations [3,4] in a nucleus. In addition quenching phenomena of stretched $6^-(\pi 1f_{7/2}, \nu 1d_{5/2}^{-1})$ states [5] excited via the ^{40}Ca$(p, n)^{40}$Sc reaction have been the subject of controversy. In order to understand these phenomena, it is necessary to obtain occupation probabilities of the nucleus—one of the most fundamental quantities in nuclear structure physics—via systematic spectroscopic studies. The $(p - f)$ shell nuclei such as the Ca isotopes stimulate much interest, since their spectroscopic structures show marked differences when compared with those of other light- and heavy-weight nuclei. The present work is designed to investigate the neutron-shell structure of the doubly closed nucleus ^{40}Ca. The occupation probabilities and the single-particle energies are obtained by the study of transfer reactions.

The one-nucleon transfer reaction is a useful tool for investigating the shell configuration in nuclei because of its simple mechanism leading to a single-hole or a single-particle state. Many researchers have studied Ca isotopes by means of (p, d) [6–8] and (d, p) [9–14] reactions as well as other unique reactions [15–17]. Most of the data, however, is not able to be used to determine occupation probabilities and single-particle energies. There are two main reasons for this. First, the entire fragmented strength was not observed due to the poor energy resolution and the narrow range of excitation energy which was measured. Secondly, there have been few studies with vector analyzing power measurements, and j^π ambiguities remain. There is a further point that needs to be noted. The precise values for these quantities relating to the shell structures depend critically on the spectroscopic factors C^2S which in turn are sensitive to a certain approximation made in the distorted-wave Born approximation (DWBA). The most uncertain term of the DWBA calculation is the form factor generated by the bound state potential of a transferred neutron. Many aspects of this problem have been discussed [18,19], and a careful normalization should be expected to yield reliable C^2S values even with a simple DWBA analysis.

In the last few years Eckle *et al.* [10,11] have performed an experimental study of the ^{40}Ca$(\vec{d}, p)^{41}$Ca reaction at 20 MeV with very high resolution. They have found and analyzed 183 levels with excitation energies of up to 8.7 MeV. As a result they concluded that the $1f_{7/2}$ orbit is completely empty and the higher $l = 1$ orbits are approximately 20% occupied. This unreasonable result may arise from difficulties in l, j assignments which occur because reactions at lower incident energies show an indistinct j dependence in the analyzing pow-

*Present address: Sony Corporation, Atsugi 243, Japan.
†Present address: Department of Intelligent Machinery and Systems, Kyushu University, Fukuoka 812, Japan.

ers. In particular, the ambiguity becomes larger as the excitation energy becomes higher. Stephenson *et al.* [20] has explained that a strong spin-orbit distortion at the higher energy incidence of 79 MeV has the effect of making larger distinctions in analyzing power for transfers of different j and the same l, though the distinctions in cross sections for different l transfers is less clear. Incidence at a slightly lower energy of about 60 MeV is expected to allow us to make reliable l, j assignments throughout a wide excitation range 0–10 MeV.

In view of the above problems, $(\vec{p}, d)$ and $(\vec{d}, p)$ reactions should be reinvestigated. Some of the authors have investigated the ^{39}Ca single-hole states up to 10-MeV excitation with the $(\vec{p}, d)$ reaction at 65 MeV [7,8]. The complementary data from the (d, p) reaction is very important to enable us to gain insight into the shell structure of ^{40}Ca, since the single-particle picture would be elucidated around the Fermi surface.

In the present paper we describe the results of a ^{40}Ca$(\vec{d}, p)^{41}$Ca reaction study. The measurements were carried out with a high quality beam of 56-MeV vector-polarized deuterons. The angular distributions of the vector-analyzing power $A_y(\theta)$ and the differential cross section $d\sigma/d\Omega(\theta)$ were measured in the energy range from the ground state to the excited states at about 10 MeV by the use of a high resolution magnetic spectrograph. The angular distribution data were analyzed by using the zero-range DWBA theory using an adiabatic approximation. For the observed levels the j^π values were deduced and the spectroscopic factors extracted. Many states were reassigned (for example, from $7/2^-$ to $5/2^-$). The shell-model structure of ^{40}Ca is discussed in regard to the valence $(2s-1d)$ and $(2p-1f)$ shells with consideration of the (p, d) data, and compared with those from recent theoretical calculations. Preliminary results on the occupation probabilities have been reported elsewhere [21].

II. EXPERIMENTAL PROCEDURE

The measurements were carried out at the Research Center for Nuclear Physics, Osaka University. Angular distributions of $d\sigma/d\Omega(\theta)$ and $A_y(\theta)$ were measured for the ^{40}Ca$(\vec{d}, p)^{41}$Ca reaction at fourteen laboratory angles between 5° and 45°. The polarized deuterons were accelerated up to 56 MeV with the AVF cyclotron, and the spin was alternated at every second. The beam current was 15 ~ 20 nA on the target. We used a self-supporting metallic foil of natural ^{40}Ca of 1.10 mg/cm^2 thickness as the target. The polarization of deuterons was measured upstream of the scattering chamber at 10-sec intervals before the (d, p) measurements were made for 90 seconds, and the vector polarization was found to be about 0.52.

The emitted protons were detected by a focal plane detector system following the spectrograph RAIDEN [22] with a solid angle of 32 msr. Two different magnetic field settings of the spectrograph were employed to cover the excitation energies 0–5 MeV and 5–10 MeV. The detector system consisted of two position sensitive proportional counters followed by a gaseous ΔE counter and a plastic E counter, which provided clear particle identification. The active range of these counters were $\geq$ 1800 mm in order to cover the focal plane completely. We used RDCs [23] to obtain position information for the protons on the focal plane. The proton momentum is expressed in terms of the focal plane position. These data were fed into a personal computer system based on a 10-MHz CPU (Intel 80286) through a status-encode module [24] which added spin information from the ion source to the position data. The detection efficiency was better than 99% during the present measurements.

III. ANALYSES

For analyses of the experimental data, zero-range DWBA calculations were carried out by using the code DWUCK [25]. Within the framework of the local energy approximation, the finite range effect of neutron-proton interaction was corrected with a parameter of 0.621 fm and the nonlocality of the optical potential with 0.85 fm and 0.54 fm for proton/neutron and deuteron, respectively.

The distorted wave was generated by the optical potential. We used an ordinary potential with a real central part of the Woods-Saxon shape, an imaginary part for volume and surface absorption, a spin-orbit potential, and a Coulomb potential. Parameters of the potentials were referred to the best-fit values for the ^{40}Ca$(\vec{p}, d)^{39}$Ca reaction at 65 MeV [7,8] by Matoba *et al.* The global potential of Menet *et al.* [26] was adopted for the proton channel. The parameters written using the usual expressions are given by

$$V = 49.9 - 0.22E_p + 26.4(N-Z)/A + 0.4ZA^{-1/3} \text{ MeV} ,$$

$$r_0 = 1.16 \text{ fm}, \quad a_0 = 0.75 \text{ fm} ,$$

$$W = 1.2 + 0.09E_p \text{ MeV} ,$$

$$W_D = 4.2 - 0.05E_p + 15.5(N-Z)/A \text{ MeV or } 0, \text{ whichever is greater} ,$$

$$r' = 1.37 \text{ fm}, \quad a' = 0.74 - 0.0008E_p + (N-Z)/A \text{ fm} ,$$

$$V_{\text{s.o.}} = 6.04 \text{ MeV}, \quad r'' = 1.064 \text{ fm}, \quad a'' = 0.78 \text{ fm} ,$$

$$r_c = 1.25 \text{ fm} .$$

Here E_p is the proton energy which varied with the excitation energy. For the deuteron channel the adiabatic potential [27] was used on the basis of Satchler's prescription [28], which was constructed with the proton and neutron potentials of Becchetti and Greenlees [29]:

$$V = 110.3 - 0.65(E_d/2) + 0.4ZA^{-1/3} \text{ MeV} ,$$

$$r_0 = 1.17 \text{ fm}, \quad a_0 = 0.779 \text{ fm} ,$$

$$W = 0.22E_d - 4.26 \text{ MeV or } 0, \text{ whichever is greater} ,$$

$$W_D = 24.8 - 0.25E_d \text{ MeV or } 0, \text{ whichever is greater} ,$$

$$r' = 1.29 \text{ fm}, \quad a' = 0.578 + 0.35(N-Z)/A \text{ fm} ,$$

$$V_{\text{s.o.}} = 4.1 \text{ fm}, \quad r'' = 1.06 \text{ fm}, \quad a'' = 0.75 \text{ fm} ,$$

$$r_c = 1.25 \text{ fm} ,$$

where E_d is the incident deuteron energy of 56 MeV. The value of $V_{\text{s.o.}}$ was reduced to $\frac{2}{3}$ [8] of the usual value of 6.2 fm to enable better fitting of $A_y(\theta)$.

For computing the form factor, the bound state wave function of captured neutron was generated as an eigenfunction of the Woods-Saxon well including the Thomas-Fermi spin-orbit potential with $\lambda = 25$. A fixed geometry of the well was used in the analyses for all transitions. Values of both the radius r_0 and the diffuseness a_0 of the well have a marked effect on transition amplitude, but little effect on the shapes of $\sigma(\theta)$ and $A_y(\theta)$. The parameters were adjusted so as to satisfy simultaneously the following: (1) the total values of C^2S should be near the sum rule, i.e., $\sum_i C^2S_i \leq 1$, for the three higher shells of $1f_{5/2}$, $2p_{3/2}$, and $2p_{1/2}$; (2) the equivalent neutron number located in the six valence $2s_{1/2}$, $1d_{3/2}$, $1f_{7/2}$, $1f_{5/2}$, $2p_{3/2}$, and $2p_{1/2}$ shells should be a total of 6–7 in the (d,p) reaction study. Under these conditions we finally determined values of $r_0 = 1.27$ fm and $a_0 = 0.67$ fm. The potential depth was calculated with the conventional well-depth procedure [30]. The binding energy of each level is given generally by the separation energy (SE) method [31,32]. The effective binding energy (EBE) method [33,34] is known to give more reasonable prescriptions for the spectroscopic factor in analyses over a wide excitation region. The EBE prescription is considered to be more reasonable especially for stripping strengths to hole states. With these two methods, however, it is impossible to analyze highly excited states beyond the neutron separation energy S_n, i.e., 8.363-MeV excitation of ^{41}Ca. When these transitions involve a large fraction of the single-particle strength, it may be possible to analyze them with unperturbed level energies for individual orbits on the basis of the EBE prescription. A harmonic oscillator potential was used to calculate the level energies. The potential depth V_{ls} was calculated by [35]

$$V_{ls} = \hbar\omega\{\Lambda + \tfrac{3}{2} + v_{ls}\, l\cdot\mathbf{s} + v_{ll}\, l(l+1)\} \text{ MeV} , \quad (1)$$

$$\hbar\omega = 41A^{-1/3} ,$$

$$v_{ls} = -20.0A^{-3/2} ,$$

$$v_{ll} = -\begin{cases} 0, & \Lambda = 0,1,2 , \\ 0.0175, & \Lambda = 3 , \\ 0.0225, & \Lambda = 4,5,6 , \\ 0.020, & \Lambda = 7,8 , \end{cases}$$

where Λ denotes the principal oscillator quantum number. The spectroscopic factor C^2S for each level was extracted with

$$\frac{d\sigma}{d\Omega} = 1.55\frac{C^2S}{2J+1}\frac{2J_f+1}{2J_i+1}\sigma_{\text{DWUCK}}(\theta) , \quad (2)$$

where J_i and J_f were the spins of the target nuclei in the entrance and exit channels of the reaction, respectively, and J was the transferred total spin.

IV. RESULTS AND DISCUSSION

Figure 1 shows an energy spectrum for the ^{40}Ca$(\vec{d},p)^{41}$Ca reaction measured at $\theta_{\text{lab}} = 11°$. The overall energy resolution is ~ 30 keV FWHM; this value is mainly due to the energy loss fluctuations in the target foil. It can be seen that the almost pure single-particle states have relatively large strengths in comparison with the two-step excitation strengths, although the strengths of two-step or compound process are enhanced at lower incident energies. Discrete levels are distributed throughout the wide excitation region. The sharp peaks appearing at the highest energy part of the spectrum, which exceeds $S_n(= 8.36$ MeV), may be long-lived resonance levels. As seen later, the angular distributions for these levels clearly exhibit a single-particle-like behavior, and hence the EBE method is appropriate for analyses of these transitions. The physical background due to, for instance, breakup protons is very small even in the highly excited region.

The spectrum data were analyzed to obtain angular distributions of $\sigma(\theta)$ and $A_y(\theta)$ by using a peak fitting code FOGRAS [36], which provided good data reduction even for spectra with complicated structures including contamination peaks. The excitation energies of levels were determined with reference to the proton momentum for the ground state transition. The errors were estimated from analyses of some known levels, and found to be within a few keV for most levels below 5-MeV excitation. Between 5 and 10 MeV the errors may be ± 10 keV.

A. Single-particle states

The single-particle states in ^{41}Ca have been investigated. We observed 91 levels up to 9.7 MeV of excitation

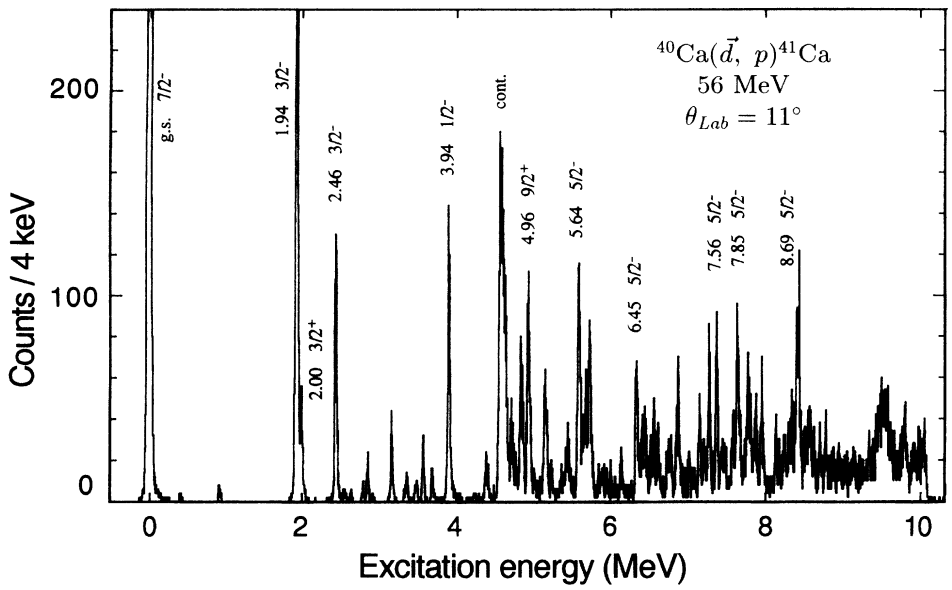

FIG. 1. Proton spectrum for the ^{40}Ca($\vec{d}$, p)^{41}Ca reaction by using 56-MeV deuterons with spin-up orientation taken at θ = 11°. The number of protons in every 4-keV energy bin is plotted versus excitation energy of ^{41}Ca. For identification, the quantum numbers and excitation energies of the typical states are given in the figure. Peaks contributed by contaminations are also identified.

energy. The quantum numbers are given for 71 states including 28 tentative assignments. Spectroscopic results of the present work are listed in Table I, and compared with those of the 20-MeV (d,p) reaction [11] by Eckle *et al.* and a review of ^{40}Ca(d,p) reaction studies [37] taking into account Eckle's data. Only the states corresponding to the present work are shown here, although Eckle *et al.* observed 183 levels up to 8.7 MeV. Low-lying states are widely acknowledged from many experimental works, and our results are consistent with these works. In the high excitation region some disagreements are seen in j^π assignments. Many levels are populated close together at $E_x > 7$ MeV, and the correspondence is not clear. The difference in excitation energies appears to be within 10 keV.

Figure 2 shows angular distributions of σ and A_y for the ground $1f_{7/2}$ state transition. The DWBA curves reasonably reproduce the experimental data. The present analysis yields a value of the spectroscopic factor of $C^2S = 0.77 \pm 0.05$. The error in the spectroscopic factor principally arises from the ambiguity in the normalization procedure [8] due to the difference in angular distribution shapes. In the present work errors were estimated using the largest and the smallest C^2S values obtained by fitting differently the DWBA curve to at least one point of the measured data in the forward region $\theta_{\rm lab} < 15°$. In Table II the present result is compared with those from previous studies on (d,p) reactions at 20 MeV [11] and 56 MeV [38], and a ^{41}Ca(e,e') reaction [16] at hundreds of MeV. The results are consistent within the experimental errors. The last column of Table II presents a quasiparticle strength [40,41] evaluated from the dispersive-mean field theory. The value of 0.75 for the $1f_{7/2}$ particle state is very close to our result. Except for the ground state, no clear $1f_{7/2}$ states are observed. Three other transitions to E_x = 5.51-, 7.39-, and 8.50-MeV levels shows angular distributions slightly resembling $1f_{7/2}$ shape. These transitions have very weak strengths and the total value $1f_{7/2}$ strength is not affected by these ambiguous assignments: almost all of the $1f_{7/2}$ strength appears to be concentrated in the ground state level. The resultant value of 0.77 indicates considerable deficiency of particles in the surface of the ^{40}Ca ground state.

The $l = 1$ transition gives rise to strong peaks in the lower energy part of the spectrum (Fig. 1). The $2p_{3/2}$ and the $2p_{1/2}$ strengths are observed at four states respectively in the range $E_x \leq 4.75$ MeV. Almost all the strengths are collected in these transitions. Angular distributions are shown in Figs. 3 and 4. The 4.10-MeV state, which was interpreted as a $5/2^+$ state previously, is reassigned as $1/2^-$, as is evident from the comparison shown in Fig. 4 (second curve from the bottom). The present C^2S values for $2p_{1/2}$ states are larger than the Eckle's values by 30$\sim$ 50%. The reason for this may be due to the different procedures used to calculate the form factors. It should be noticed that the cross section calculations for $1/2^-$ transitions show the poorest agreement for any class of transitions in the present work, and the errors of these values are somewhat large. At the higher region of E_x=6.9–9.5 MeV few very weak states have been tentatively assigned for each transition, and Eckle *et al.* observed four or five very weak transitions at E_x=5.0–6.4 MeV. The assignments for these states are ambiguous, but it has little effect on the total strength.

The $l = 3$ strength is widely distributed into many states for E_x=6–10 MeV, which arises almost exclusively from the $j = 5/2$ transfer. It is notable that the clear peaks arising in this energy region are mainly attributed to the $l = 3, j = 5/2$ strength. The $1f_{5/2}$ assignments are given to 18 levels definitely and eight levels tentatively below S_n. Above S_n, five definite states and one tentative are observed. Angular distributions are displayed in Fig. 5 for twelve typical transitions. The large negative amplitude of A_y is sufficient evidence to show that these are $l = 3, j = 5/2$ transitions. As can be seen in Table I, six states are reassigned definitely in this work, which were interpreted in terms of $1f_{7/2}$ by Eckle *et al.* Most of the other $5/2^-$ assignments agree with Eckle's results.

TABLE I. Level structure of ^{41}Ca from ^{40}Ca(d,p) reaction.

Present results				Ref. [11]			Ref. [37]	
No.	E_x (MeV)	J^π	C^2S	No.	E_x (MeV)	J^π	E_x (MeV)	J^π
1	Ground state	7/2−	0.77	1	Ground state	7/2−	Ground state	7/2−
2	1.9401	3/2−	0.54	2	1.9427	3/2−	1.94261	3/2−
3	2.0073	3/2+	0.14	3	2.0098	3/2+	2.0098	3/2+
4	2.4613	3/2−	0.20	4	2.4626	3/2−	2.4622	3/2−
5	2.5743			5	2.5742	5/2−	2.5479	5/2−
6	2.6701	1/2+	0.084	7	2.6705	1/2+	2.6699	1/2+
7	2.8851			8	2.8842	9/2+	2.8835	7/2+
8	2.9570			9	2.9598		2.9594	7/2−
9	3.0512	(3/2+	0.092)	10	3.0504		3.0497	3/2(−)
10	3.2011	9/2+	0.0083	11	3.2004	9/2+	3.20124	9/2+
11	3.3497			12	3.3682		3.6964	11/2+
12	3.4004	1/2+	0.12	13	3.3998	1/2+	3.3999	1/2+
13	3.4955			14	3.4945	5/2+	3.4948	5/2+
14	3.5270	3/2+	0.038	15	3.5260	5/2+	3.5257	3/2+
15	3.6147	1/2−	0.092	16	3.6135	1/2−	3.6135	1/2−
16	3.657						3.6764	9/2−
17	3.7303	3/2−	0.027	17	3.7303	3/2−	3.7304	3/2−
18	3.8455	1/2+	0.076	19	3.8457	1/2+	3.8454	1/2+
19	3.9432	1/2−	0.57	21	3.9439	1/2−	3.9441	1/2−
20	4.1090	1/2−	0.035	24	4.0933	(5/2)+	4.0943	6/2+
21	4.224							
22	4.295							
23	4.338							
24	4.4463	9/2+	0.0074	28	4.4485	9/2+	4.4485	9/2+
25	4.559			29	4.5206			
26	5.6017	3/2−	0.14	30	4.6029	3/2−	4.6031	3/2−
27	4.7543	1/2−	0.29	32	4.7534	1/2−	4.7526	1/2−
28	4.8177	3/2+	0.035	34	4.8171	5/2+	4.8157	5/2+
29	4.8773	5/2−	0.091	36	4.8783	(5/2)−	4.8783	5/2−
30	4.9692	9/2+	0.029	37	4.9705	9/2+	4.9705	9/2+
31	5.0215	(1/2+	0.17)	39	5.0136	1/2+	5.0116	1/2+
32	5.0545	(1/2+	0.11)	40	5.0469	(9/2)+	5.0469	(7/2,9/2)+
33	5.0718			41	5.0723	1/2−	5.0723	1/2−
34	5.1890	9/2+	0.029	47	5.1949	9/2+	5.1949	9/2+
35	5.2743			49	5.2833	(5/2)+	5.2833	5/2+
36	5.3573							
37	5.4037	(1/2−	0.028)	55	5.4517	1/2−	5.4517	1/2−
38	5.4621			56	5.4689	3/2−	5.4688	3/2−
39	5.5128	(7/2−	0.0027)	59	5.5199	(5/2)−	5.5199	(5/2,7/2)−
		(5/2−	0.0072)					
40	5.6431	5/2−	0.12	63	5.6488	(5/2)−	5.6488	(5/2,7/2)−
41	5.7071			66	5.7040	1/2−	5.7040	1/2−
42	5.7477	(9/2+	0.011)	69	5.7509	9/2+	5.7509	9/2+
		(5/2−	0.0081)	70	5.7596	(5/2+)	5.7596	(3/2,5/2)+
43	5.7974	5/2−	0.081	71	5.8012	(5/2)−	5.8012	(5/2,7/2)−
44	6.0714			81	6.0833	(3/2)+	6.083	(3/2,5/2)+
45	6.2407	5/2−	0.017	89	6.2388	5/2−	6.2388	5/2−
				97	6.4379	5/2−	6.4379	5/2−
46	6.4525	5/2−	0.061	98	6.4507	5/2−	6.4507	5/2−
47	6.5311	5/2−	0.035	100	6.5206	5/2−	6.5206	
48	6.5712	5/2−	0.037	101	6.5674	7/2−	6.5674	7/2−
49	6.6527	5/2−	0.015	105	6.6470	5/2−	6.647	5/2−
50	6.6990	5/2−	0.031	107	6.6862	7/2−	6.6862	7/2−
51	6.7587	5/2−	0.024	109	6.7481	7/2−	6.7481	7/2−
52	6.8845	5/2−	0.016	114	6.8695	(5/2)−		
		(3/2−	0.0010)	116	6.9173	(9/2)+		
53	6.9337							
54	7.0298	(9/2+	0.025)	119	7.0148	(9/2)+		

TABLE I. *(Continued).*

Present results				Ref. [11]			Ref. [37]	
No.	E_x (MeV)	J^π	C^2S	No.	E_x (MeV)	J^π	E_x (MeV)	J^π
55	7.1136			122	7.0731	1/2−		
56	7.1897	(3/2−	0.0013)					
		(9/2+	0.015)					
57	7.2585	(1/2−	0.0035)					
		(5/2−	0.0032)					
58	7.3315	5/2−	0.032	133	7.3084	7/2−		
59	7.3959	(5/2−	0.0091)	136	7.3771	(5/2)−		
		(7/2−	0.0047)	137	7.3929			
60	7.4598	5/2−	0.050	139	7.4373	5/2−		
61	7.5239							
62	7.5666	5/2−	0.049	144	7.5379	(5/2)−		
63	7.6362	(5/2−	0.012)	146	7.6076	(9/2)+		
64	7.6846							
65	7.7337							
66	7.7945	5/2−	0.021	154	7.8171	5/2−		
67	7.8510	5/2−	0.052	155	7.8878	5/2−		
68	7.8944	5/2−	0.014	156	7.9191	5/2−		
69	7.9491	5/2−	0.012	157	7.9568	5/2−		
70	7.9953	(5/2−	0.015)	158	7.9741	5/2−		
71	8.1053	5/2−	0.029	162	8.1018	7/2−		
72	8.1957	5/2−	0.031	167	8.1977	7/2−		
		Neutron separation energy 8.363 MeV						
73	8.397	5/2−	0.018					
74	8.458	(9/2+	0.0014)	175	8.4474	(9/2)+		
75	8.509	(7/2−	0.0058)	177	8.5224	7/2−		
76	8.547			179	8.549	5/2−		
77	8.573							
78	8.621	5/2−	0.021	180	8.6196	5/2−		
79	8.697	5/2−	0.077	181	8.6378	5/2−		
80	8.783	5/2−	0.025					
81	8.855	(9/2+	0.0025)					
82	8.916	(9/2+	0.0006)					
		(3/2−	0.0011)					
83	8.997	(9/2+	0.0020)					
84	9.084	5/2−	0.020					
85	9.177							
86	9.273	(5/2−	0.0010)					
		(9/2+	0.0006)					
87	9.315							
88	9.367							
89	9.414							
90	9.475							
91	9.545							

It is found that the strength of the $1f_{5/2}$ transition is shared somewhat equally by many levels, since the shell orbit is located at higher energies than the other $(p-f)$ orbits from a shell model consideration.

Four strong peaks appearing at the excitation range from 3.2 to 5.2 MeV in the spectrum are ascribed to the $l=4, j=9/2$ transition angular distributions displayed in Fig. 6. The $1g_{9/2}$ assignments for these states are confirmed. The values of C^2S are very small; this is because the unperturbed level is located at a much higher energy than the $1f_{5/2}$ orbit. The $1g_{9/2}$ strength

TABLE II. Spectroscopic factor for the ground $1f_{7/2}$ state in ^{41}Ca.

(d,p)[a] 56 MeV	(d,p)[b] 20 MeV	(d,p)[c] 56 MeV	(e,e')[d]	DMF[e]
0.77±0.05	0.85	0.75	0.83±0.05	0.75

[a]Present work.
[b]Eckle *et al.* [11].
[c]Hatanaka *et al.* [38].
[d]Platchkov *et al.* [16].
[e]Quasiparticle strength with dispersive-mean field theory [40].

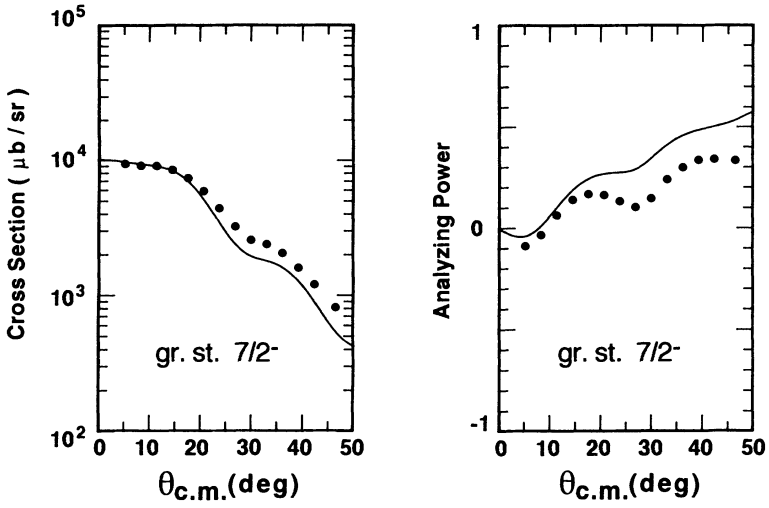

FIG. 2. Angular distributions of differential cross sections (left) and analyzing powers (right) for transition to the ground $1f_{7/2}$ state via the ^{40}Ca$(\vec{d},p)^{41}$Ca reaction at 56 MeV. Solid lines represent DWBA predictions. The calculated cross section is normalized to the experimental as described in the text.

is shared by many transitions, and only a fraction of the total strength appears to have been found. Very weak strengths are observed in the region $E_x \geq 6$ MeV of the spectrum and five states are tentatively assigned in the unbound region. More missing strengths exist.

The strippings on $1d_{3/2}$ and $2s_{1/2}$ hole states have been widely observed for the low excitation region. At higher excitations no definite strengths are observed in the region studied presently. The population of the states in the lower energy region has been interpreted as an indication that these two shells are not completely filled, since the $2d$ and the $3s$ strength are not the likely assignment from the shell model systematics. The deviation from a double magic shell configuration has been an attractive subject regarding the ground state of ^{40}Ca.

Angular distributions of the $l = 2, j = 3/2$ transfers are

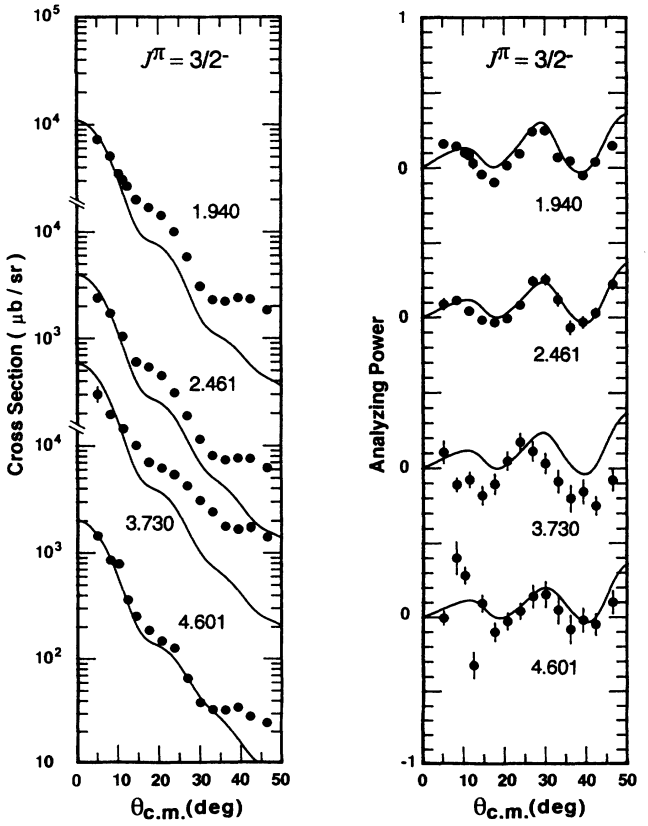

FIG. 3. The same as Fig. 2, but the $2p_{3/2}$ states. Data points of the peak contributed by contaminations are omitted. The excitation energies are given in the figure.

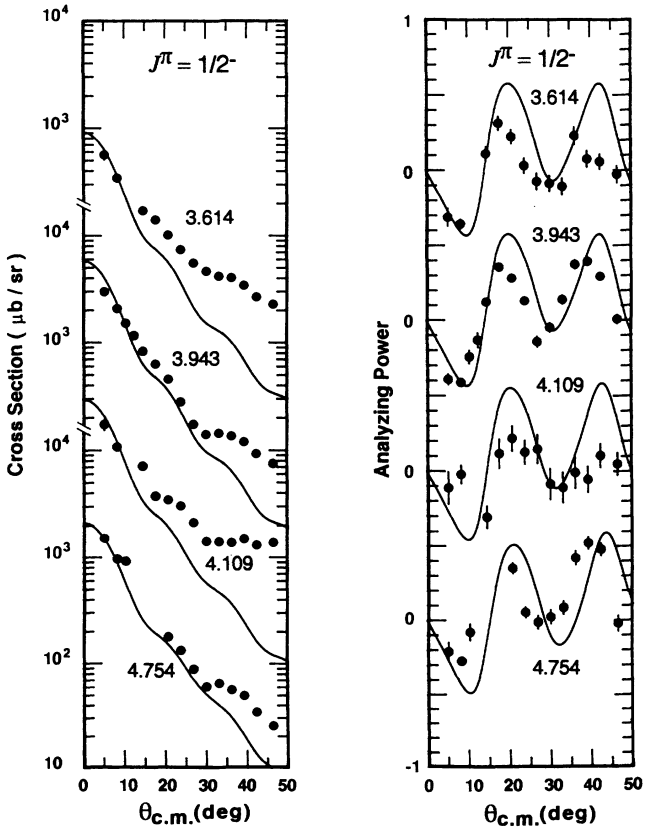

FIG. 4. The same as Fig. 2, but for the $2p_{1/2}$ states. Data points of the peak contributed by contaminations are omitted. The excitation energies are given in the figure.

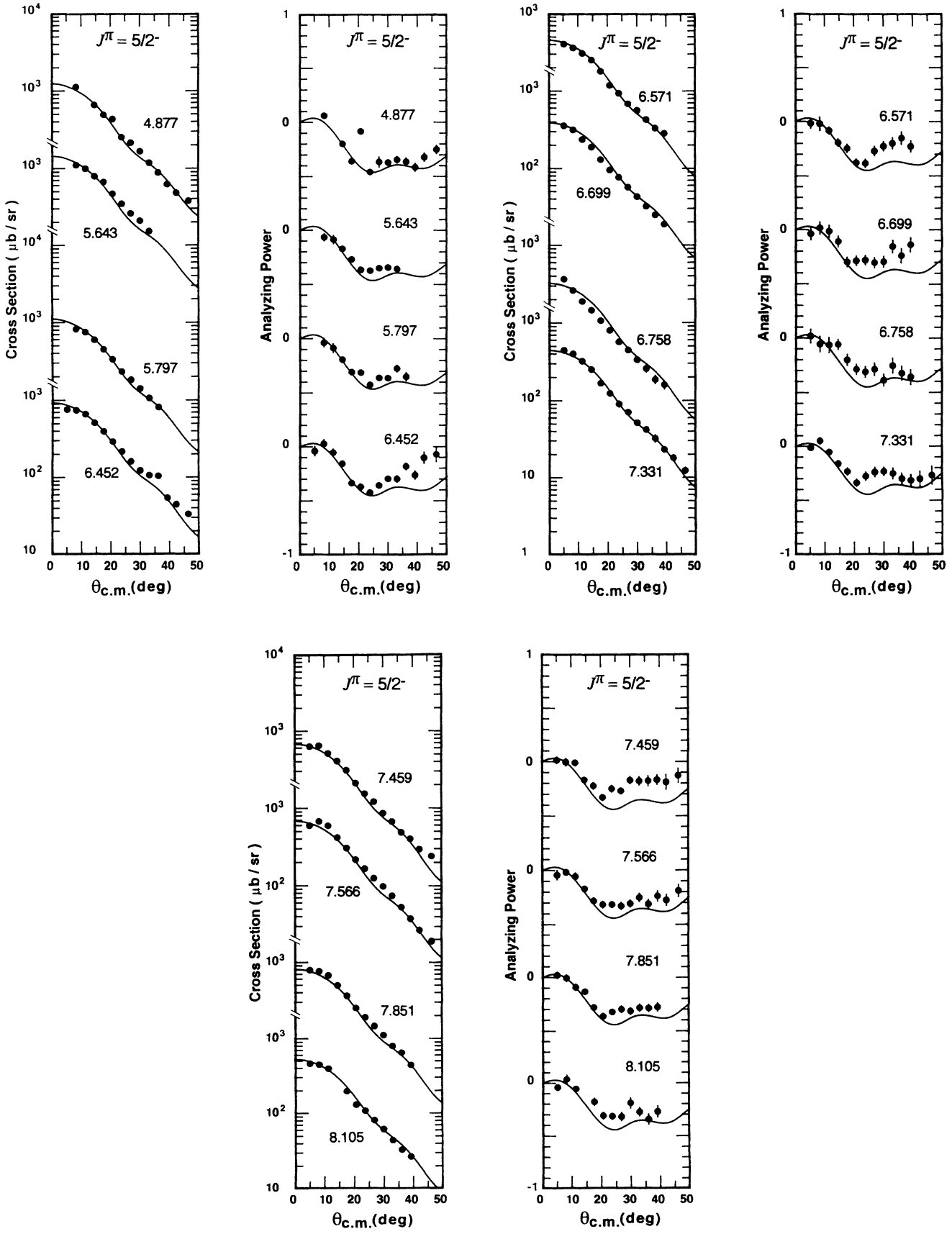

FIG. 5. The same as Fig. 2, but for the $1f_{5/2}$ states. Data points of the peak contributed by contaminations are omitted. The excitation energies are given in the figure.

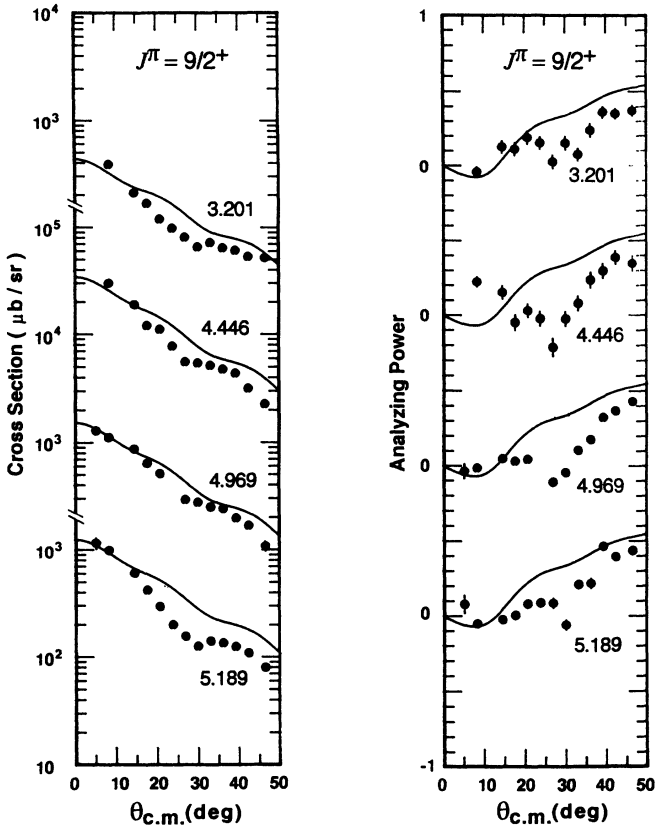

FIG. 6. The same as Fig. 2, but for the $1g_{9/2}$ states. Data points of the peak contributed by contaminations are omitted. The excitation energies are given in the figure.

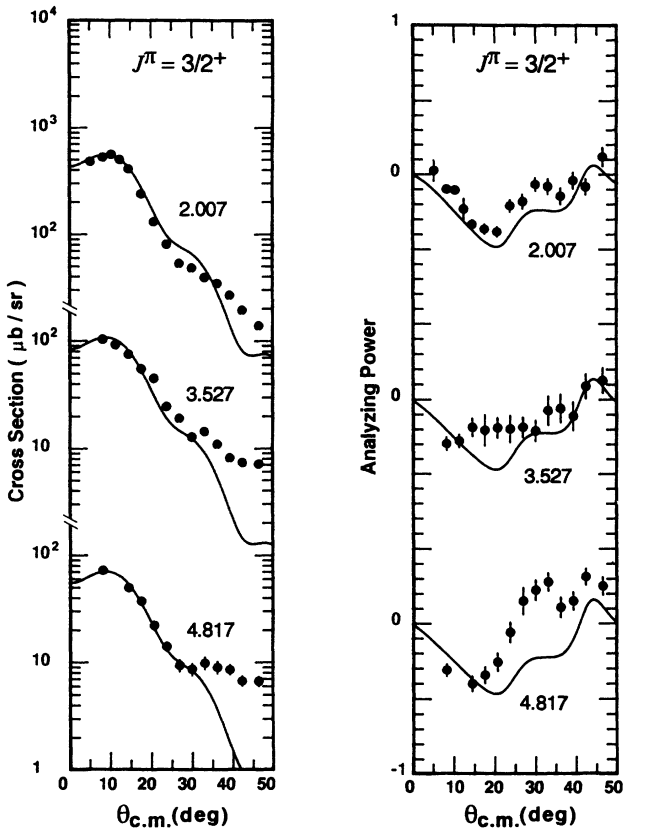

FIG. 7. The same as Fig. 2, but for the $1d_{3/2}$ states. Data points of the peak contributed by contaminations are omitted. The excitation energies are given in the figure.

displayed in Fig. 7. They are reproduced by DWBA calculations with reasonable differences. Accompanied by a tentative assignment four $1d_{3/2}$ strengths are observed. The 3.52- and 4.81-MeV states were reassigned. Previously, they have been explained as $1d_{5/2}$ states, but we have found no $1d_{5/2}$ strengths throughout the measured region. There have been several estimates of the absolute value of C^2S for the lowest hole $1d_{3/2}$ state at 2.01 MeV. Typical values are presented in Table III. With the source term method Pinkston, Philpott and Satchler [39] found a value of C^2S=0.16 for a 12-MeV (d,p) reaction. Eckle *et al.* obtained $C^2S = 0.17$ with a quasiparticle-phonon coupling calculation and $C^2S = 0.06$ by using the ordinary well-depth analysis with the SE prescription. For the stripping on the orbit below the Fermi surface, greater C^2S values are always given with a more realistic form factor [39] than with the ordinary prescription. We have extracted a spectroscopic factor of $C^2S = 0.14 \pm 0.02$, which is close to the former results. The agreement for this state and, as discussed before, for the ground state indicates that rather realistic C^2S values can be obtained simply by a careful normalization in the DWBA calculation under the EBE method.

The $l = 0$ transitions are found for five states of E_x=2.67–5.05 MeV in ^{41}Ca. Figure 8 presents the angular distributions for the lowest three $2s_{1/2}$ states. Previous assignments are confirmed from the agreement with DWBA curves. For excitation at around 5 MeV, the $2s_{1/2}$ assignments have been ambiguous. The shape of $A_y(\theta)$ is similar to that of $l = 0$ transfer, but the $\sigma(\theta)$ shape is rather structureless at $\theta_{\rm lab} < 11°$. This may imply only a slight contribution of single-particle strength, and in fact spectroscopic factors resulted in unreasonably large values.

B. Occupation probability and single-particle energy

In principle, the total strength $\sum C^2S$ for the stripping (d,p) reaction directly measures the emptiness u^2 of the shell orbit. The present results are listed in the first column of Table IV. In the third column, the values for the ^{40}Ca$(p,d)^{39}$Ca reaction [8], which measure the fullness v^2 of the shell, are listed.

TABLE III. Spectroscopic factor for the 2.01-MeV $1d_{3/2}$ state in ^{41}Ca.

(d,p)[a] 56 MeV	(d,p)[b] 20 MeV	(d,p)[c] 12 MeV	Theory[d]
0.14±0.02	0.06	0.16	0.17

[a]Present work, analyzed with the EBE method.
[b]Eckle *et al.* [11], with the ordinary WD method.
[c]Pinkston *et al.* [39], with the source term method.
[d]Quasiparticle-phonon coupling calculation [11].

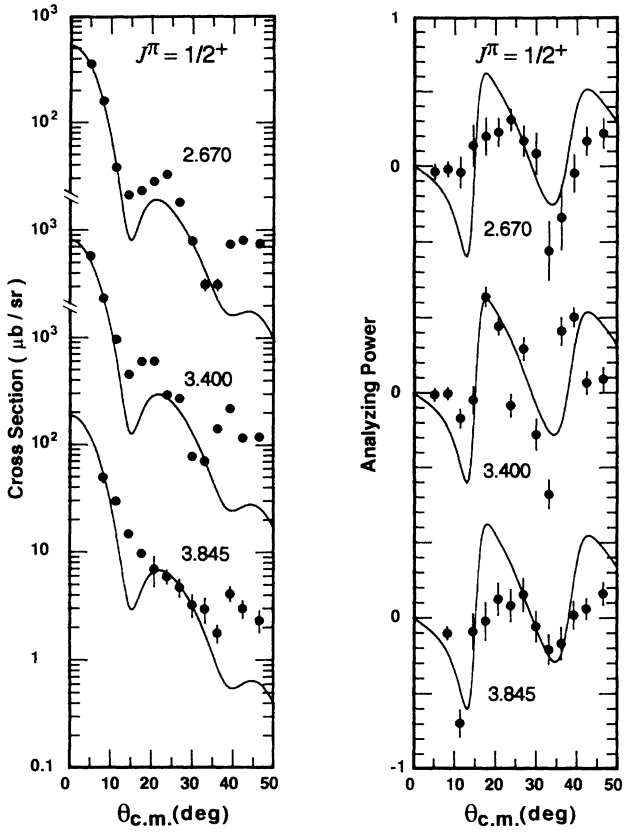

FIG. 8. The same as Fig. 2, but for the $2s_{1/2}$ states. Data points of the peak contributed by contaminations are omitted. The excitation energies are given in the figure.

If single-particle and single-hole strengths are assumed to undergo a quasiparticle excitation of the ^{40}Ca ground state $|\tilde{0}\rangle$, then we can express the excited states in ^{41}Ca and ^{39}Ca by the following expressions:

$$|^{41}\mathrm{Ca};\ j \text{ particle}\rangle = a_j^\dagger|\tilde{0}\rangle \ ,$$

$$|^{39}\mathrm{Ca};\ j \text{ hole}\rangle = \tilde{a}_j|\tilde{0}\rangle \ .$$

The spectroscopic amplitude $\mathcal{S}$ is then given by

$$\mathcal{S} = \begin{cases} \langle^{41}\mathrm{Ca};\ j|c_j^\dagger|\tilde{0}\rangle = u & \text{for } (d,p) \\ \langle^{39}\mathrm{Ca};\ j|c_j|\tilde{0}\rangle = v & \text{for } (p,d) \end{cases}$$

where $c^\dagger$ is the linear combination

$$c_j^\dagger = ua_j^\dagger + v\tilde{a}_j \ .$$

Consequently we obtain

$$u^2 + v^2 = 1 \ . \tag{3}$$

The fifth column of Table IV gives summed values of emptiness and fullness. The difference between these values and Eq. (3) is about 10–20 %, which is a larger deviation than the experimental accuracy. This suggests that the BCS theory is not applicable for medium-heavy nuclei having a magic shell such as the ^{40}Ca nucleus. The total strength of (d,p) reaction corresponds to the strength of the quasiparticle excitation [40], which is listed in the sixth column of Table IV. These values are very close to those of the present work.

The (d,p) reaction should yield occupation probabilities of a shell-orbit via the BCS theory, i.e., $1 - \sum C^2S$. The resultant values for six valence shells are listed in Table V with theoretical estimates from the dispersive-mean field [40] and the extended second-RPA [42] calculations. The present values predict a greater deviation from a magic shell than the theories. However, it must be noted that the BCS theory is poorly applicable to the ^{40}Ca nucleus. More reasonable values would be obtained by averaging the empirical expectations from the ^{40}Ca$(p,d)^{39}$Ca and the ^{40}Ca$(d,p)^{41}$Ca, since the effect of the residual nuclear wave functions would be counteracted by each other. This is based on an assumption that the asymmetry of structure between ^{39}Ca and ^{41}Ca is not very large. The results are listed in the second column of Table V. This experimental prediction, shown in the second column, is in better quantitative agreement with the values derived from the theories.

The single-particle energy $E_{nlj}^{\mathrm{s.p.}}$ is also an important quantity for investigating the shell structure. Following

TABLE IV. Summed strength $\sum C^2S$ and centroid energy $\bar{E}$ for the valence shells from ^{40}Ca(d,p) and ^{40}Ca(p,d) reaction. Fifth column is the sum of emptiness (first column) and fullness (third column). The last two columns are theoretical expectations for particle (p) and hole (h) strengths in^{40}Ca.

	(d,p)[a] 56 MeV		(p,d)[b] 65 MeV			Strength[c]	
Orbit	$\sum C^2S$	$\bar{E}$ (MeV)	$\frac{\sum C^2S}{(2j+1)}$	$\bar{E}$ (MeV)	Sum	p	h
$1f_{5/2}$	0.97	6.98				0.92	
$2p_{1/2}$	0.98	4.16				0.89	
$2p_{3/2}$	0.90	2.50	0.02	4.54	0.92	0.85	
$1f_{7/2}$	0.77	0	0.04	3.19	0.81	0.75	
$1d_{3/2}$	0.21	2.33	0.93	0	1.14		0.78
$2s_{1/2}$	0.28	3.30	0.88	2.65	1.16		0.81

[a]Present work.
[b]Reference [8].
[c]Quasiparticle strength with the dispersive-mean field theory [40].

TABLE V. Occupation probability and single-particle energy for the valence shells in ^{40}Ca nucleus.

	Occupation probability				Single-particle energy (MeV)	
Orbit	(d,p)[a]	Mean[b]	DMF[c]	ESRPA[d]	Present[e]	DMF[f]
$1f_{5/2}$	0.03	0.03	0.07	0.06	−1.38	−1.50
$2p_{1/2}$	0.02	0.02	0.07	0.03	−4.20	−4.19
$2p_{3/2}$	0.10	0.06	0.08	0.03	−5.86	−5.59
$1f_{7/2}$	0.23	0.13	0.12	0.06	−8.36	−8.54
$1d_{3/2}$	0.79	0.86	0.89	0.89	−15.64	−15.79
$2s_{1/2}$	0.72	0.80	0.91	0.92	−18.29	−17.53

[a]Present data, given by $1-\sum C^2S$.
[b]Mean values of occupations from (d,p) and (p,d).
[c]Dispersive-mean field theory [40].
[d]Extended second RPA [42].
[e]Present work described in the text.

the procedure given in Ref. [40], one can obtain the experimental energies for the valence single-particle states with respect to the Fermi energy E_F. The energies $E^{\text{s.p.}}_{nlj}$ above E_F are scaled using the centroid energy $\overline{E_{nlj}}$ of the stripping reaction, and the energies $E^{\text{s.p.}}_{nlj}$ below E_F are scaled by that of the pickup reaction. The centroid energy $\overline{E_{nlj}}$ is given by

$$\overline{E_{nlj}} = \frac{\sum C^2S \cdot E_x}{\sum C^2S} \ .$$

The centroid energies are shown in Table IV. Here we chose single-particle energies for the nearest shells to the Fermi surface:

$$E^{\text{s.p.}}_{1f_{7/2}} = S_n(^{41}\text{Ca}) \ ,$$

$$E^{\text{s.p.}}_{1d_{3/2}} = S_n(^{40}\text{Ca}) \ .$$

The single-particle energies are listed in Table V, together with the predictions of the dispersive-mean field theory [40]. They are found to be in good agreement with each other. By using these energies, the BCS solution is not obtained even with a greater pairing force $G = 30/A$ because of the wide particle-hole gap > 7 MeV. This supports the previously mentioned limitation of the BCS theory for the ^{40}Ca shell structure.

V. CONCLUSION

The single-particle levels in the ^{41}Ca nucleus have been investigated by means of the ^{40}Ca$(\vec{d},p)$ reaction at 56 MeV. The data were analyzed by the DWBA calculations using an adiabatic approximation. Transferred angular momenta l,j were deduced definitely for 43 levels, and tentatively for 28 levels up to 9.7 MeV of excitation. The data of analyzing power for this incident energy enables us to make reliable assignments throughout the whole excitation range, and many states were reassigned in the present work. The spectroscopic factors C^2S were extracted using an effective binding energy prescription. We obtained the values $C^2S = 0.77 \pm 0.05$ and 0.14 ± 0.02 for the ground $1f_{7/2}$ and the lowest hole $1d_{3/2}$ state, respectively, and agreement with referenced values was confirmed. The occupation probabilities and the single-particle energies in ^{40}Ca were discussed for the valence shells $2p_{1/2}$, $2p_{3/2}$, $1f_{5/2}$, $1f_{7/2}$, $1d_{3/2}$, and $2s_{1/2}$. The present results for these quantities are consistent with recent predictions of the dispersive-mean field and the extended second RPA theory.

ACKNOWLEDGMENTS

The authors are indebted to the staff of the Research Center for Nuclear Physics (RCNP), Osaka University, especially to Professor H. Ikegami, for their continuous encouragement of this study. This work was performed under the program numbers 26E15 and 29A16 at RCNP.

[1] B. D. Anderson, J. N. Knudson, P. C. Tandy, J. W. Watson, R. Madey, and C. C. Foster, Phys. Rev. Lett. **45**, 699 (1980).
[2] C. N. Papanicolas *et al.*, Phys. Rev. Lett. **58**, 2296 (1987).
[3] V. R. Pandharipande, C. N. Papanicolas, and J. Wambach, Phys. Rev. Lett. **53**, 1133 (1984).
[4] M. Jaminon, C. Mahaux, and H. Ngô, Nucl. Phys. **A440**, 228 (1985).
[5] T. Chittrakarn *et al.*, Phys. Rev. C **34**, 80 (1986).
[6] P. Martin, M. Buenerd, Y. Dupont, and M. Chabre, Nucl. Phys. **A185**, 465 (1972).
[7] M. Matoba, H. Ijiri, H. Ohgaki, S. Uehara, T. Fujiki, Y. Uozumi, H. Kugimiya, N. Koori, I. Kumabe, and M. Nakano, Phys. Rev. C **39**, 1658 (1989).
[8] M. Matoba, O. Iwamoto, Y. Uozumi, T. Sakae, N. Koori, T. Fujiki, H. Ohgaki, H. Ijiri, T. Maki, and M. Nakano, Phys. Rev. C **48**, 95 (1993).
[9] T. A. Belote, A. Sperduto, and W. W. Buechner, Phys. Rev. **139**, B80 (1965).
[10] F. J. Eckle, H. Lenske, G. Eckle, G. Graw, R. Hertenberger, H. Kader, F. Merz, H. Nann, P. Schiemenz, and H. H. Wolter, Phys. Rev. C **39**, 1662 (1989).
[11] F. J. Eckle *et al.*, Nucl. Phys. **A506**, 159 (1990).

[12] E. Kashy, A. Sperduto, H. A. Enge, and W. W. Buechner, Phys. Rev. **135**, B865 (1964).
[13] W. D. Metz, W. D. Callender, and C. K. Bockelman, Phys. Rev. C **12**, 827 (1975).
[14] R. Abegg, J. D. Hutton, and M. E. Williams-Norton, Nucl. Phys. **A303**, 121 (1978).
[15] J. W. Watson, M. Ahmad, D. W. Devins, B. S. Flanders, D. L. Friesel, N. S. Chant, P. G. Roos, and J. Wastell, Phys. Rev. C **26**, 961 (1982).
[16] S. Platchkov *et al.*, Phys. Rev. Lett. **61**, 1465 (1988).
[17] G. J. Kramer *et al.*, Phys. Rev. B **227**, 199 (1989).
[18] J. S. Winfield, N. A. Jelly, W. D. M. Rae, and C. L. Woods, Nucl. Phys. **A437**, 65 (1985).
[19] M. C. Radhakrishna, N. G. Puttaswamy, H. Nann, D. W. Miller, P. P. Singh, W. W. Jacobs, W. P. Jones, and E. J. Stephenson, Phys. Rev. C **40**, 1603 (1989).
[20] E. J. Stephenson, V. R. Cupps, J. A. Tostevin, R. C. Johnson, J. D. Brown, C. C. Foster, W. P. Jones, D. W. Miller, H. Nann, and P. Schwandt, Nucl. Phys. **A469**, 467 (1987).
[21] Y. Uozumi, S. Widodo, H. Ijiri, T. Sakae, M. Matoba, T. Maki, M. Nakano, and N. Koori, Contribution to 7th International Conference on Polarization Phenomena in Nuclear Physics, Paris, 1990, p. 82B, unpublished.
[22] H. Ikegami, S. Morinobu, I. Katayama, M. Fujiwara, and S. Yamabe, Nucl. Instrum. Methods **175**, 33 (1980).
[23] H. Ohgaki, H. Ijiri, T. Sakae, N. Koori, and M. Matoba, IEEE Trans. Nucl. Sci. **NS-34** (1987).
[24] T. Sajima, R. Kubo, N. Motomura, S. Widodo, H. Kugimiya, T. Fujii, Y. Uozumi, H. Ohgaki, H. Ijiri, M. Matoba, T. Sakae, and N. Koori, Engi. Sci. Rep. Kyushu Univ. **11**, 33 (1989) [in Japanese].
[25] P. D. Kunz, code DWUCK, University of Colorado (unpublished).
[26] J. J. H. Menet, E. E. Gross, J. J. Malanify, and A. Zucker, Phys. Rev. C **4**, 1114 (1971).
[27] R. C. Johnson and P. J. R. Soper, Phys. Rev. C **1**, 976 (1970).
[28] G. R. Satchler, Phys. Rev. C **4**, 1485 (1971).
[29] F. P. Becchetti, Jr. and G. W. Greenlees, Phys. Rev. **182**, 1990 (1969).
[30] G. R. Satchler, *Nuclear Direct Reactions* (Clarendon, Oxford, 1983), p. 715.
[31] W. T. Pinkston and G. R. Satchler, Nucl. Phys. **72**, 641 (1965).
[32] R. J. Philpott, W. T. Pinkston, and G. R. Satchler, Nucl. Phys. **A119**, 241 (1968).
[33] N. Austern, Phys. Rev. **136**, B1743 (1964).
[34] R. L. Kozub, Phys. Rev. **172**, 1078 (1968).
[35] A. Bohr and B. Mottelson, *Nuclear Structure* (Benjamin, New York, 1969), Vol. II, p. 464.
[36] S. Matsuki, code FOGRAS, Kyoto University (unpublished).
[37] P. M. Endt, Nucl. Phys. **A521**, 1 (1990).
[38] K. Hatanaka, N. Matsuoka, T. Saito, K. Hosono, M. Kondo, S. Kato, T. Higo, S. Matsuki, Y. Kadota, and K. Ogino, Nucl. Phys. **A419**, 530 (1984).
[39] W. T. Pinkston, R. J. Philpott, and G. R. Satchler, Nucl. Phys. **A125**, 176 (1969).
[40] C. H. Johnson and C. Mahaux, Phys. Rev. C **38**, 2589 (1988).
[41] C. Mahaux and R. Sartor, Nucl. Phys. **A528**, 253 (1991).
[42] S. Nishikzaki, S. Drozdz, J. Wambach, and J. Speth, Phys. Lett. B **215**, 231 (1988).